Experimental verification of rank 1 chaos in switch-controlled Chua circuit

Ali Oksasoglu,[1,a)] Serdar Ozoguz,[2,b)] Ahmet S. Demirkol,[2,c)] Tayfun Akgul,[2,d)] and Qiudong Wang[1,e)]
[1]*Department of Mathematics, The University of Arizona, Tucson, Arizona 85721, USA*
[2]*Faculty of Electrical-Electronics Engineering, Istanbul Technical University, 34469 Istanbul, Turkey*

(Received 23 September 2008; accepted 31 December 2008; published online 12 February 2009)

In this paper, we provide the first experimental proof for the existence of rank 1 chaos in the switch-controlled Chua circuit by following a step-by-step procedure given by the theory of rank 1 maps. At the center of this procedure is a periodically kicked limit cycle obtained from the unforced system. Then, this limit cycle is subjected to periodic kicks by adding externally controlled switches to the original circuit. Both the smooth nonlinearity and the piecewise linear cases are considered in this experimental investigation. Experimental results are found to be in concordance with the conclusions of the theory. © *2009 American Institute of Physics*. [DOI: 10.1063/1.3073967]

This paper is about experimentally demonstrating the use of a new chaos theory, namely, the theory of rank 1 maps, in practical systems. One of the most important practical implications of the theory is that it provides a recipelike procedure to obtain chaos from a weakly stable limit cycle. The setting of the theory is easily satisfied by use of externally controlled switches in a given autonomous system. The practical system used in this investigation is the well-known Chua circuit. Our investigation in this paper has shown that the predictions of the theory are in great agreement with our experimental findings. Thus, it can reasonably be claimed that this theory can provide a practical means of generating chaos from many practical electronic oscillators.

I. INTRODUCTION

In a sequence of papers published recently, Oksasoglu and co-workers proposed a generic scheme of creating rank 1 chaos in practical circuits by using periodically controlled switches.[1–4] In these studies, the theory of rank 1 maps was applied to rigorously verify the existence of rank 1 attractors. In addition, extensive numerical simulations were conducted in search of the strange attractors implicated under the guidance of the theory. The results of these numerical simulations were found to be in perfect match with the conclusions of the theory. The theory of rank 1 maps used in these studies is a new chaos theory developed in recent years by Wang and Young.[5–7] This new chaos theory is based on the Jakobson theory on quadratic maps[8] and the studies of Benedicks and Carleson on strongly dissipative Hénon maps.[9]

In this paper, we provide the first experimental evidence of rank 1 chaos in a switch-controlled circuit, namely, the switch-controlled Chua circuit[10] as proposed by Oksasoglu and Wang in Ref. 4. To demonstrate the applicability of the theory of the rank 1 maps, a Hopf limit cycle in the smooth case and an arbitrary limit cycle in the piecewise linear (PWL) case are used in this investigation. Since a local nonlinearity is needed to create Hopf bifurcations, a Chua circuit with a nonlinear resistor of cubic nonlinearity is constructed following the procedure outlined in Ref. 11. Then, the parameters of the circuit are so chosen that it has a weakly stable oscillation coming out of a supercritical Hopf bifurcation. For the case of arbitrary (non-Hopf) limit cycles, a local nonlinearity is not necessary; hence, the use of the original Chua circuit with a three-segment PWL resistor is sufficient for this purpose. In both cases, once a limit cycle is created, switches controlled by externally applied periodic pulses are added to the circuit in such a way as to modulate the state variables, namely, the capacitor voltages and the inductor current.

The addition of the periodically controlled switches to an existing nonlinear system provides a natural setting for the application of the theory of rank 1 maps. In other words, the use of periodically controlled switches generates the kicking effect proposed by Wang and Young[7,12] to create rank 1 chaos. Consequently, in the range of parameters where the theory of rank 1 maps applies, strange attractors do appear in such a way as predicted by the theory.

A great majority of the existing studies on chaotic attractors are based on breaking the homoclinic loop by small perturbations to yield a transverse homoclinic orbit (transversal intersections of the stable and unstable manifolds) in the phase space (see, e.g., Ref. 13). The rank 1 attractors presented in this paper are, however, of a different kind. They are generated by small disturbances that are periodically applied to a weakly stable limit cycle. When small disturbances in the form of periodic kicks are introduced (by use of externally controlled switches in this case), the shape of the weakly stable limit cycle is slightly deformed. Then, the natural force of shearing created by the nonlinearity of the original system goes to work and exaggerates the initial deformation to create chaos. The dynamical properties of the rank 1 attractors created that way are dominated by the so-

[a)]Electronic mail: alioksas@email.arizona.edu. Also at Honeywell Inc., Tucson, AZ 85737.
[b)]Electronic mail: ozoguz@itu.edu.tr.
[c)]Electronic mail: demirkola@itu.edu.tr.
[d)]Electronic mail: tayfun.akgul@itu.edu.tr.
[e)]Electronic mail: dwang@math.arizona.edu.

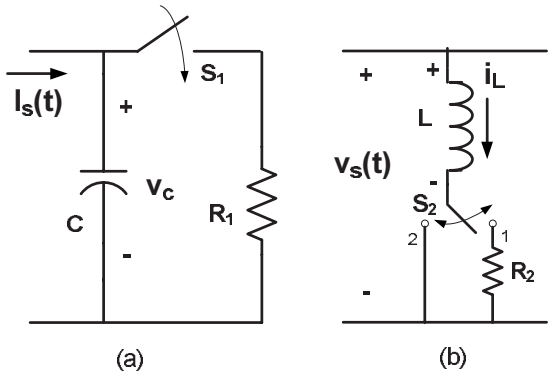

FIG. 1. A switch-controlled state variable modulation scheme.

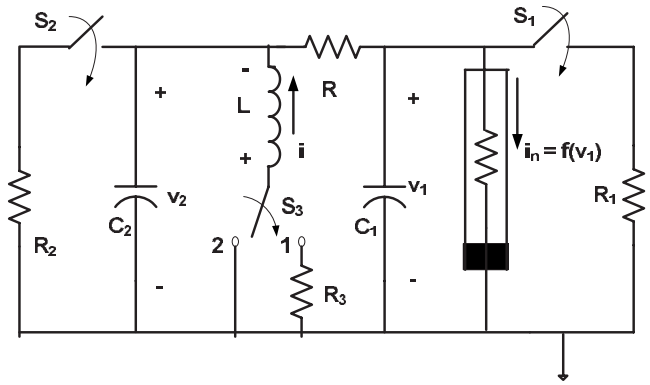

FIG. 2. Switched-controlled Chua circuit.

called Sinai–Ruelle–Bowen measures[14] representing the statistical law of the system.

It is worth noting that the use of various kicking schemes in the study of chaotic dynamics is not uncommon.[15–17] However, the study of the strange attractors in this paper differs from others in that it is supported by a comprehensive theory of dynamics that has a long history. The theory itself is little known outside the pure mathematical side of the dynamical systems community and has only been recently developed into a form that is applicable to concrete systems of differential equations. We refer the reader to a recent tutorial paper for more background information on the theory and its potential applications to circuits and systems.[18]

II. THEORETICAL SETTING AND IMPLEMENTATION APPROACH

In this section, we briefly discuss the setting of the theory and a practical approach originally introduced in Ref. 4 to generically satisfy the requirements of the theory. We first start with an autonomous system given by

$$\frac{d\mathbf{u}}{dt} = f_\mu(\mathbf{u}), \tag{1}$$

where $\mathbf{u} \in \mathbb{R}^n$, $n \geq 2$, represents the system state variables and $\mu \in \mathbb{R}^m$, $m \geq 1$, the system parameters. It is assumed that there is a $\mu = \mu_0$ at which the system of Eq. (1) goes through a supercritical Hopf bifurcation. This system is then modified to obtain the nonautonomous system of the form

$$\frac{d\mathbf{u}}{dt} = f_\mu(\mathbf{u}) + \varepsilon \Phi(\mathbf{u}) P_{T,p}(t), \tag{2}$$

where $P_{T,p}(t)$ is a periodic pulse train with a pulse width of p and a period of T, $\Phi(\mathbf{u})$ is a function that determines the shape of the forcing, and ε is used to control the magnitude of the forcing. Let $T \gg p$ so that a pulse of pulse width p is followed by a long relaxation period $T-p$. We regard the system of Eq. (2) as the kicked version of the system of Eq. (1). When the system of Eq. (1) is an electrical circuit whose state variables are the capacitor voltages and inductor currents, the system of Eq. (2) can be implemented for certain $\Phi(\mathbf{u})$ by modulating the state variables through switches externally controlled by $P_{T,p}(t)$. This scheme, depicted in Fig. 1, was proposed by Oksasoglu and Wang in Ref. 4. In Fig. 1, each switch is controlled by the periodic pulse train $P_{T,p}(t)$.

In this case, the governing equations for the capacitor voltage and the inductor current are given by

$$\begin{aligned} C\frac{dv_c}{dt} &= i_s(t) - v_c G_1 P_{T,p}(t), \\ L\frac{di_L}{dt} &= v_s(t) - i_L R_2 P_{T,p}(t). \end{aligned} \tag{3}$$

In the scheme of Fig. 1, the resulting $\Phi(\mathbf{u})$, the shape of the forcing, becomes $\Phi(\mathbf{u}) = -\mathbf{u}$.

III. SWITCH-CONTROLLED CHUA CIRCUIT

For the experimental investigations of this paper, we apply the above-outlined scheme to the well-known Chua circuit.[10] The modified circuit, which is referred to as the switch-controlled Chua circuit, is depicted in Fig. 2. The switches $\mathbf{S}_i$ are controlled by a periodic pulse train with p_0 and T_0 being the physical pulse width and the period, respectively.

A. Smooth case

Due to the need for a local nonlinearity for Hopf bifurcations to occur, the PWL resistor (Chua's diode) in the circuit of Fig. 2 is replaced with a nonlinear resistor whose $v-i$ characteristic is given by

$$i_n(v_1) = g(v_1) = a_1 v_1 + a_3 v_1^3. \tag{4}$$

The physical implementation of this cubic nonlinearity is achieved by using the design approach given in Ref. 11. The governing equations for the switch-controlled circuit can be given by

$$\begin{aligned} C_1\frac{dv_1}{dt} &= G(v_2 - v_1) - g(v_1) - G_1 v_1, \\ C_2\frac{dv_2}{dt} &= i + G(v_1 - v_2) - G_2 v_2, \quad L\frac{di}{dt} = -v_2 - R_3 i \end{aligned} \tag{5}$$

for $nT_0 \leq t < nT_0 + p_0$ and by

$$C_1\frac{dv_1}{dt} = G(v_2 - v_1) - g(v_1),$$

$$C_2\frac{dv_2}{dt} = i + G(v_1 - v_2), \quad L\frac{di}{dt} = -v_2 \tag{6}$$

for $nT_0+p_0 \le t < (n+1)T_0$, $n=0,1,2,\ldots$. Putting Eqs. (5) and (6) together, we obtain

$$C_1\frac{dv_1}{dt} = G(v_2 - v_1) - g(v_1) - G_1 v_1 \sum_{n=0}^{\infty} F_{n,p_0,T_0}(t),$$

$$C_2\frac{dv_2}{dt} = i + G(v_1 - v_2) - G_2 v_2 \sum_{n=0}^{\infty} F_{n,p_0,T_0}(t), \tag{7}$$

$$L\frac{di}{dt} = -v_2 - R_3 i \sum_{n=0}^{\infty} F_{n,p_0,T_0}(t),$$

where

$$F_{n,T_0,p_0}(t) = \begin{cases} 1, & nT_0 \le t < nT_0 + p_0 \\ 0, & \text{elsewhere.} \end{cases} \tag{8}$$

By setting

$$x = \frac{v_1}{V_0}, \quad y = \frac{v_2}{V_0}, \quad z = \frac{i}{I_0}, \quad t \to \frac{t}{\omega_n} \tag{9}$$

we obtain the following dimensionless set of equations:

$$\frac{dx}{dt} = \alpha[y - h(x)] - \varepsilon_1 x P_{T,p}(t),$$

$$\frac{dy}{dt} = \gamma[x - y + \rho z] - \varepsilon_2 y P_{T,p}(t), \tag{10}$$

$$\frac{dz}{dt} = -\beta y - \varepsilon_3 z P_{T,p}(t),$$

where

$$P_{T,p}(t) = \frac{1}{p}\sum_{n=-\infty}^{\infty} F_{n,T,p}(t), \quad h(x) = b_1 x + b_3 x^3,$$

$$p = p_0\omega_n, \quad T = T_0\omega_n, \quad b_1 = 1 + \frac{a_1}{G}, \quad b_3 = \frac{a_3 V_0^2}{G},$$

$$\alpha = \frac{G}{C_1\omega_n}, \quad \gamma = \frac{G}{C_2\omega_n} = 1.0, \quad \rho = \frac{R}{R_n}, \quad R_n = \frac{V_0}{I_0}, \tag{11}$$

$$\beta = \frac{R_n}{L\omega_n}, \quad \varepsilon_1 = \frac{\alpha R p}{R_1}, \quad \varepsilon_2 = \frac{\gamma R p}{R_2}, \quad \varepsilon_3 = \frac{\rho\beta R_3 p}{R}.$$

B. Conditions for Hopf bifurcation and rank 1 chaos

In this subsection, the conditions for the Hopf limit cycle and rank 1 chaos are derived. These conditions are obtained by following an explicit, recipe-like procedure given in Ref. 4 and give the values of parameters for the system of Eq. (10), for which rank 1 chaos is likely to occur. For this purpose, first, we consider the autonomous part of the system of Eq. (10) and look for the values of parameters for a supercritical Hopf bifurcation at $(x,y,z)=(0,0,0)$. For the computations to follow, the parameter ρ is regarded as the bifurcation parameter. Observe that at

$$\rho_0 = -\frac{\alpha(b_1 - 1)(\alpha b_1 + 1)}{\beta} > 0, \tag{12}$$

the eigenvalues of the linear part of Eq. (10) are $\pm i\omega$ and $-(\alpha b_1 + 1)$, where

$$\omega^2 = -\alpha^2 b_1(b_1 - 1) > 0. \tag{13}$$

Thus, a necessary condition for a Hopf bifurcation to occur is

$$b_1 \in (0,1). \tag{14}$$

According to the standard theory of Hopf bifurcations, Eq. (10) has a center manifold, on which the equation for the flow can be transformed into the following normal form:

$$\frac{dz}{dt} = (a(\mu) + \omega(\mu)\sqrt{-1})z + k_1(\mu)z^2\bar{z} + k_2(\mu)z^3\bar{z}^2 + \cdots, \tag{15}$$

where $k_1(\mu)$, $k_2(\mu)$ are complex numbers. The fact that there is a well-defined computational process to reach the indicated normal form is important to us. Let us write

$$k_1(\mu) = -E(\mu) + F(\mu)\sqrt{-1}. \tag{16}$$

From the computations given in Ref. 4, we have

$$E(0) = -c_1(1 + 2\alpha b_1 - \alpha), \quad F(0) = -c_1\frac{\omega}{\alpha b_1}(1 + 2\alpha b_1), \tag{17}$$

where

$$c_1 = \frac{-3\alpha b_3}{8b_1(1 + 2b_1\alpha + b_1\alpha^2)}. \tag{18}$$

Furthermore, in order to have a weakly stable periodic solution coming out of the origin, it is also necessary to have $E(0)>0$ yielding

$$\frac{-3\alpha b_3}{8b_1(\alpha^2 b_1 + 2\alpha b_1 + 1)}[1 + 2\alpha b_1 - \alpha] < 0. \tag{19}$$

Consequently, for a supercritical Hopf limit cycle to occur, we must have

$$b_1 > \frac{\alpha - 1}{2\alpha} \text{ if } b_3 > 0, \quad b_1 < \frac{\alpha - 1}{2\alpha} \text{ if } b_3 < 0. \tag{20}$$

As was shown in Ref. 12, in order for rank 1 attractors to exist, a relatively large *twist* number, as defined below, is needed,

$$\tau := \left|\frac{F(0)}{E(0)}\right|. \tag{21}$$

Therefore, to find rank 1 attractors, the values of parameters are adjusted in such a way to make the following large:

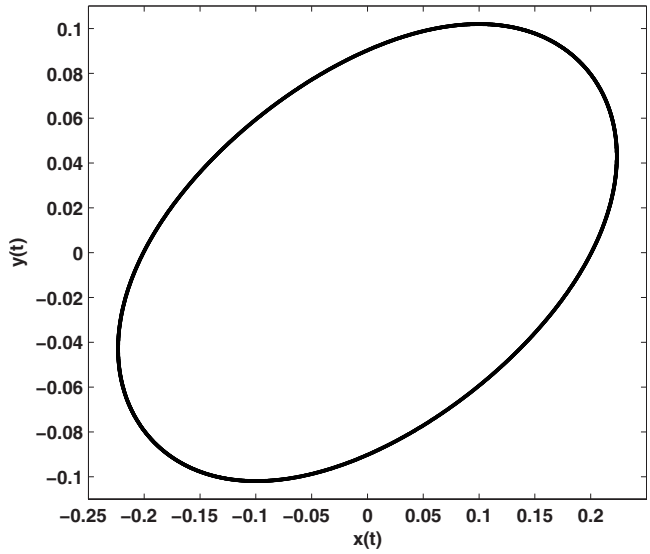

FIG. 3. A Hopf limit cycle from numerical simulations ($\varepsilon_i=0$).

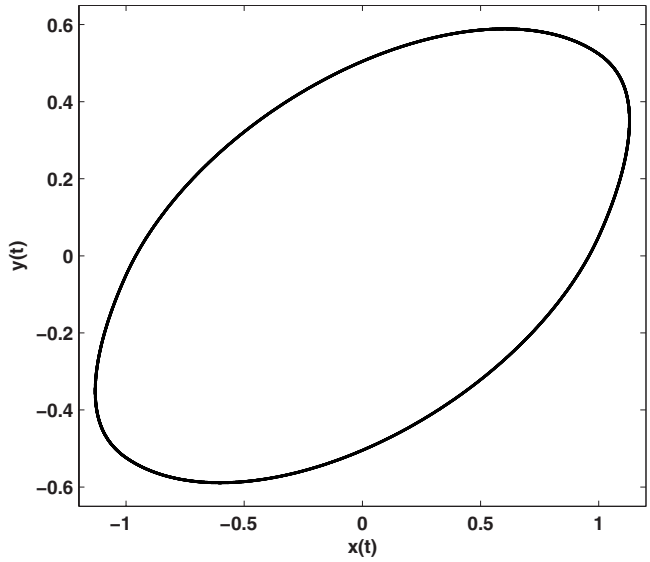

FIG. 4. A non-Hopf limit cycle from numerical simulations ($\varepsilon_i=0$).

$$\left|\frac{F(0)}{E(0)}\right| = \left|\frac{\mathrm{Im}(k_1)}{\mathrm{Re}(k_1)}\right| = \left|\frac{\omega(1+2\alpha b_1)}{\alpha b_1(1+2\alpha b_1-\alpha)}\right|. \tag{22}$$

In summary, the values of parameters are determined using the following guidelines as given in Ref. 18: Let α, β, γ, ρ, b_1, b_3 be the parameters of the autonomous part of Eq. (10) and p, $\varepsilon=\varepsilon_1$, T be the parameters of the periodic forcing. The values of all parameters except T are fixed as follows:

(i) *Parameter values for Hopf bifurcation:* $b_3\neq 0$, $\beta>0$, $\alpha>1$ are arbitrarily fixed, and ρ is around $\rho_0=-\alpha(b_1-1)(\alpha b_1+1)/\beta$.
(ii) *Strong shearing:* choose $b_1\in(0,1)$ sufficiently close to $b_1=(\alpha-1)/2\alpha$ either from above or below depending on the sign of b_3 [see Eq. (20) for stability criterion].
(iii) *Parameters of forcing:* choose ε relatively small, e.g., $\varepsilon<1$.

With the guidance of the steps above, the following parameter values are chosen and fixed:

$$\alpha=2.0,\quad \beta=2.0,\quad \gamma=1.0,\quad b_3=-1.0,\quad b_1=0.242,$$
$$\rho_0=1.124\,872,\quad \rho=\rho_0-0.005. \tag{23}$$

A Hopf limit cycle numerically obtained for the values of Eq. (23) is shown in Fig. 3. This is the limit cycle that is going to be kicked to obtain rank 1 chaos. In this case, the twist constant is roughly

$$\tau := \left|\frac{F(0)}{E(0)}\right| = 108. \tag{24}$$

C. Piecewise linear case

In this case, the $v-i$ characteristics of the nonlinear resistor of Fig. 2 is given by

$$i_n(v_1)=g(v_1)=G_b v_1+0.5(G_a-G_b)(|v_1+V_b|-|v_1-V_b|). \tag{25}$$

Using the change of variables given in Eq. (9) results in the same dimensionless system as that of Eq. (10):

$$\frac{dx}{dt}=\alpha[y-h(x)]-\varepsilon_1 x P_{T,p}(t),$$
$$\frac{dy}{dt}=\gamma[x-y+\rho z]-\varepsilon_2 y P_{T,p}(t), \tag{26}$$
$$\frac{dz}{dt}=-\beta y-\varepsilon_3 z P_{T,p}(t).$$

However, in this case, the nonlinear function $h(x)$ is given by

$$h(x)=m_1+0.5(m_0-m_1)(|x+B_p|-|x-B_p|), \tag{27}$$

where

$$m_0=1+\frac{G_a}{G},\quad m_1=1+\frac{G_b}{G},\quad B_p=\frac{V_b}{V_0}. \tag{28}$$

The rest of the system parameters are as given by Eq. (11). The autonomous part of Eq. (26), obtained by setting $\varepsilon_1=\varepsilon_2=\varepsilon_3=0$, has a limit cycle, as shown in Fig. 4, for

$$(\alpha,\gamma,\beta,\rho,m_0,m_1,B_p)=(2.0,1.0,2.0,1.12,-0.75,-0.225,1.0). \tag{29}$$

This limit cycle is the one that is kicked to obtain rank 1 chaos.

IV. NUMERICAL SIMULATIONS FOR RANK 1 CHAOS

In this section, the results of our numerical simulations for both smooth and PWL cases are presented. Although various single- or multiswitch control schemes can be formulated by setting selected ε_i to zero, in our investigations, only $\mathbf{S_1}$ and $\mathbf{S_2}$ are employed by setting $\varepsilon_3=0$. The numerical results of this section are obtained by directly solving Eqs.

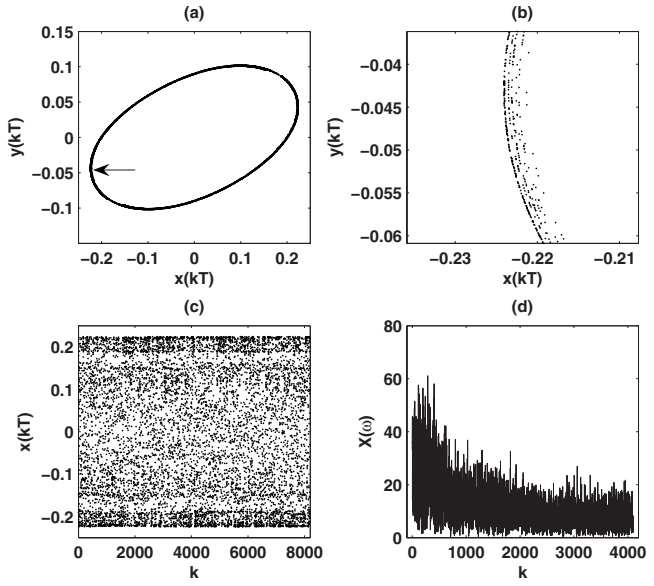

FIG. 5. A single-switch case rank 1 attractor from numerical simulations: smooth case ($\varepsilon_1=0.5$, $\varepsilon_2=\varepsilon_3=0$, $T=501.5$). (a) Time-T map on x-y plane. (b) Magnification of the indicated area in (a). (c) Time evolution of x_k. (d) Frequency spectrum of x_k.

(10) and (26). Computations are performed using the fourth-order Runge–Kutta routine starting at $t_0=0$. For both cases, only the kicking parameters (ε_i and T) are varied to obtain rank 1 chaos. The remaining system parameters are fixed as given in Eq. (23) for the smooth case (Hopf limit cycle) and Eq. (29) for the PWL case. For each chaotic picture presented, the time-T map obtained for one discrete orbit starting near the attractor is given along with the time evolution and the frequency spectrum of the attractor.

A. Hopf limit cycle

The rank 1 attractors presented in this subsection are numerically obtained for different parameter values and kicking schemes. The limit cycle kicked in this case is the Hopf limit cycle shown in Fig. 3. The attractor of Fig. 5(a) is obtained by employing only $\mathbf{S_1}$ with $\varepsilon_1=0.5$ and $T=501.5$. In this case, a high value of T is used to capture the true rank 1 nature of the attractor. Even though the attractor in Fig. 5(a) appears to be a simple closed curve, it is, in fact, a chaotic attractor of a very complicated structure. This complicated structure is evident from Fig. 5(b), which is the magnification of the indicated area in Fig. 5(a) and the continuous characteristic of the frequency spectrum shown in Fig. 5(d). For more on this, we refer the reader to Ref. 18.

Using lower values of T reveals more of the chaotic structure of the attractors. The attractors in the next two figures, Figs. 6 and 7, are such examples for the single-switch ($\mathbf{S_1}$) and the double-switch ($\mathbf{S_1}$ and $\mathbf{S_2}$) cases, respectively. The parameter values used in these cases are $\varepsilon_1=0.5$ and $T=97$ for Fig. 6 and $\varepsilon_1=0.5$, $\varepsilon_2=0.34$, and $T=87.5$ for Fig. 7. As stated before, with lower values of T, the chaotic structure of these attractors is readily visible.

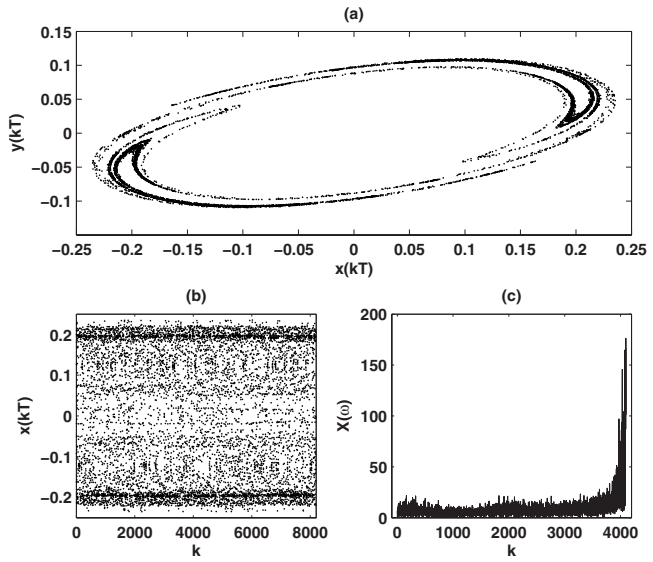

FIG. 6. A single-switch case rank 1 attractor from numerical simulations: smooth case ($\varepsilon_1=0.5$, $\varepsilon_2=\varepsilon_3=0$, $T=97.0$). (a) Time-T map on x-y plane. (b) Time evolution of x_k. (c) Frequency spectrum of x_k.

B. Arbitrary limit cycle

In this subsection, the rank 1 attractors shown in Figs. 8–10 are numerically obtained by kicking the non-Hopf limit cycle given in Fig. 4. The approach taken in presenting the figures of this subsection is the same as that of Sec. IV A. In other words, the attractor depicted in Fig. 8 is for the single-switch ($\mathbf{S_1}$) scheme with a large value of T, and those of Figs. 9 and 10 are for lower T values with the single-switch ($\mathbf{S_1}$) and double-switch ($\mathbf{S_1}$ and $\mathbf{S_2}$) kicking schemes, respectively. The parameter values used in these cases are $\varepsilon_1=0.5$ and $T=253$ for Fig. 8, $\varepsilon_1=0.5$ and $T=71.5$ for Fig. 9, and $\varepsilon_1=0.36$, $\varepsilon_2=0.17$, and $T=72$ for Fig. 10. As before, for the cases of lower T (Figs. 9 and 10), the arms of the attractors are readily visible, whereas for the case of large T (Fig. 8),

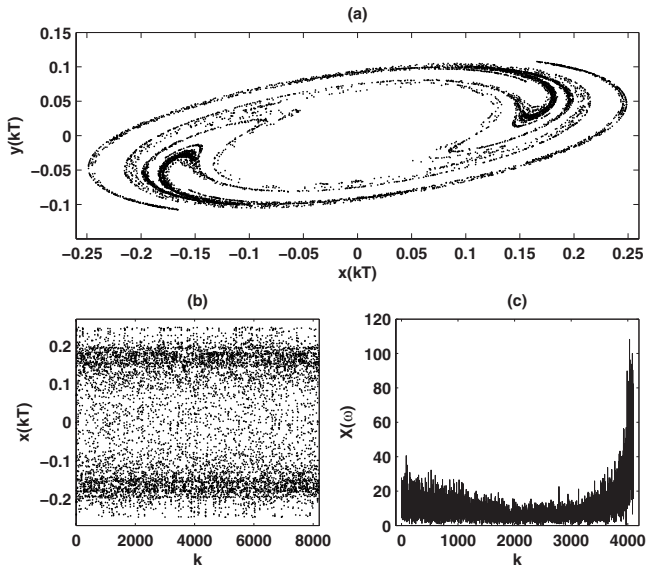

FIG. 7. A two-switch case rank 1 attractor from numerical simulations: smooth case ($\varepsilon_1=0.5$, $\varepsilon_2=0.34$, $\varepsilon_3=0$, $T=87.5$). (a) Time-T map on x-y plane. (b) Time evolution of x_k. (c) Frequency spectrum of x_k.

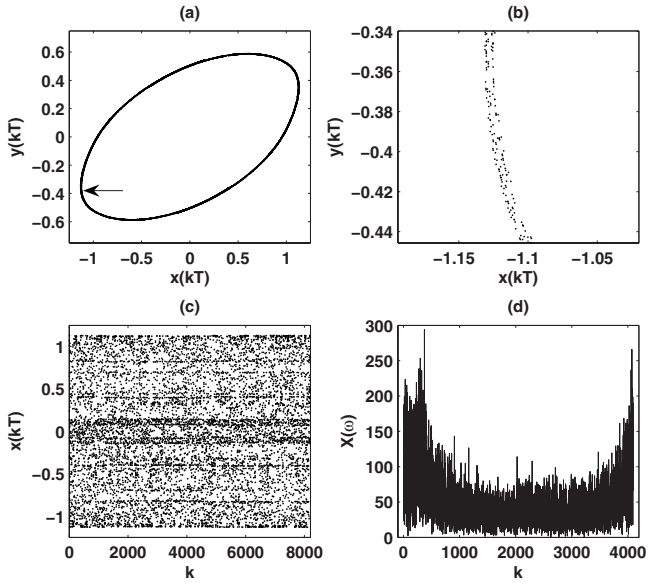

FIG. 8. A single-switch case rank 1 attractor from numerical simulations: PWL case ($\varepsilon_1=0.5$, $\varepsilon_2=\varepsilon_3=0$, $T=253$). (a) Time-T map on x-y plane. (b) Magnification of the indicated area in (a). (c) Time evolution of x_k. (d) Frequency spectrum of x_k.

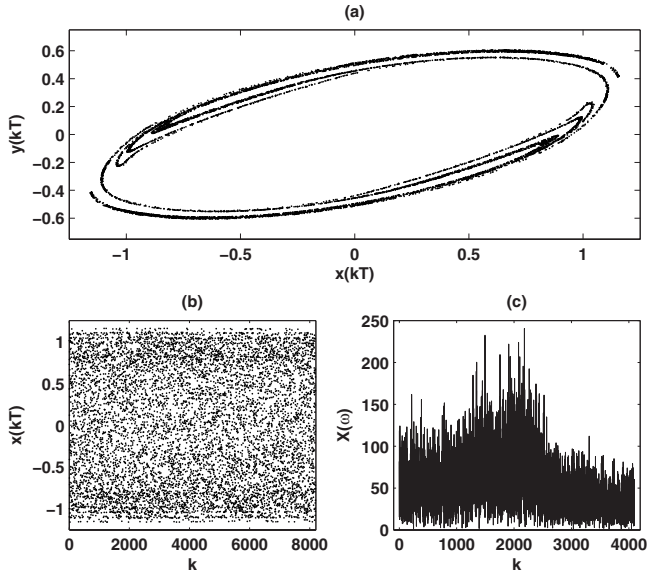

FIG. 10. A two-switch case rank 1 attractor from numerical simulations: PWL case ($\varepsilon_1=0.36$, $\varepsilon_2=0.17$, $\varepsilon_3=0$, $T=72$). (a) Time-T map on x-y plane. (b) Time evolution of x_k. (c) Frequency spectrum of x_k.

they are radially pushed down to give the attractor the appearance of a simple closed curve, whose complicated structure is also evident from Figs. 8(b) and 8(d).

V. CIRCUIT IMPLEMENTATION AND EXPERIMENTAL RESULTS

In this section, the circuit implementations and the experimental results for both the smooth and PWL cases are presented. For both cases, the circuit of Fig. 2 is realized with different implementations for the nonlinear resistor. In the smooth case, the nonlinear resistor is implemented to realize a $v-i$ characteristic of the form $i=a_1v_1+a_3v_1^3$. In the PWL case, its implementation realizes a three-segment PWL $v-i$ characteristic. The passive element values in both cases are chosen to be

$$C_1=2.2\ \text{nF},\quad C_2=4.4\ \text{nF},\quad L=5\ \text{mH},\quad R=1.5\ \text{k}\Omega. \tag{30}$$

With the values above, the frequency scaling constant is found to be

$$\omega_n=\frac{1}{RC_2}=151\,515\ \text{rad/s}, \tag{31}$$

resulting in the following nondimensional parameter values:

$$\alpha=2.0,\quad \gamma=1.0,\quad \beta=1.98. \tag{32}$$

In addition, the pulse width of the kicking pulse train is chosen to be $p_0=3.5\ \mu$s, giving $p=p_0\omega_n=0.523$.

As before, for both cases, three experimentally obtained rank 1 attractors are presented. As in the case of numerical simulations, the first two of these figures are for the single-switch case, one with a high and another with a low value of T. The third figure is for the double-switch case with a low value of T. Note that $T=\omega_nT_0$ where T_0 is the period of the kicking pulse train. In the single-switch scheme, only the switch $\mathbf{S_1}$ is activated. In the case of double-switch scheme, the switches $\mathbf{S_1}$ and $\mathbf{S_2}$ both are activated. In these experimental simulations, first, the values of ε_1 and ε_2 (for the double-switch scheme only) are fixed. This is accomplished by fixing the values of R_1 and R_2 in Fig. 2. Then, to generate chaotic attractors, only the period T_0 (i.e., T) of the kicking pulse train is varied. As in the case of numerical simulations, the time-T maps of the experimentally obtained chaotic attractors are given in the figures to follow. This is achieved by sampling the experimentally obtained flow of the system (circuit of Fig. 2) every T_0 seconds.

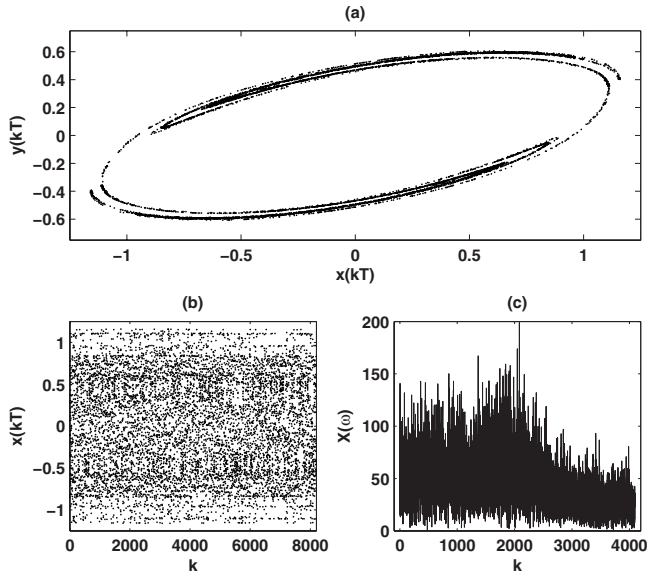

FIG. 9. A single-switch case rank 1 attractor from numerical simulations: PWL case ($\varepsilon_1=0.5$, $\varepsilon_2=\varepsilon_3=0$, $T=71.5$). (a) Time-T map on x-y plane. (b) Time evolution of x_k. (c) Frequency spectrum of x_k.

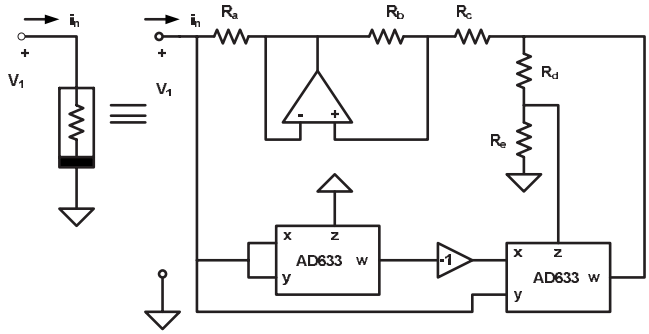

FIG. 11. Cubic resistor implementation.

A. Smooth case

The circuit implementation of the cubic $v-i$ characteristic, $i_n=a_1v_1+a_3v_1^3$, of the nonlinear resistor in Fig. 2 can be accomplished by use of analog multipliers. Here, the same design approach given in Ref. 11 is followed. The specific analog multipliers used for this purpose are AD633 of Analog Devices. For operational amplifiers, AD711 are used. The biasing used for all of the active elements is ±5 V. The resulting implementation of this cubic $v-i$ characteristic is given in Fig. 11. For the controlled switches of Fig. 2, Texas Instruments' CD4016 is used.

In order to stay in the vicinity of the normalized parameter values given in Eq. (23), the physical element values for Fig. 11 are chosen to be

$$R_a = R_b = R_d = R_e = 2.2\ \text{k}\Omega, \quad R_c = 2.07\ \text{k}\Omega. \tag{33}$$

These values result in the following nondimensional parameter values:

$$b_1 = 0.242, \quad b_3 = -1.0, \quad \rho = 1.12. \tag{34}$$

With this choice of parameter values, an experimentally obtained Hopf limit cycle is shown in Fig. 12. In Fig. 12, the horizontal axis corresponds to $v_1(t)$ of Fig. 2 with 0.5 V/div and the vertical axis to $v_2(t)$ of Fig. 2 with 0.25 V/div. This Hopf limit cycle is the one that is kicked to experimentally obtain the rank 1 attractors given in this subsection.

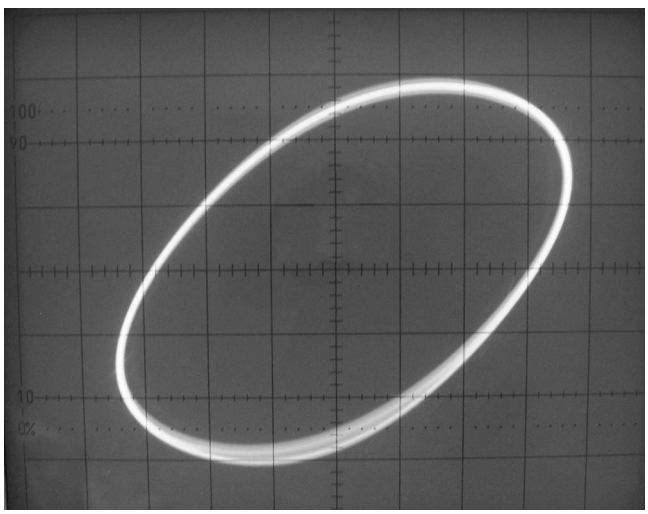

FIG. 12. A Hopf limit cycle from experimental simulations ($\varepsilon_i=0$).

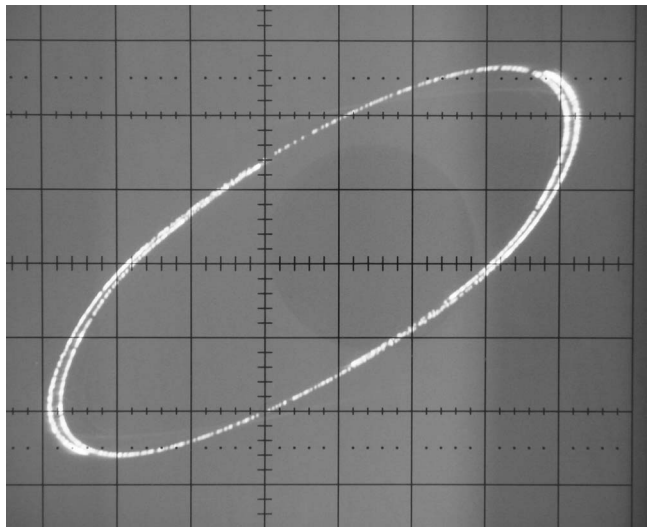

FIG. 13. Time-T map for a single-switch case rank 1 attractor from experimental simulations: smooth case ($\varepsilon_1=0.787$, $\varepsilon_2=\varepsilon_3=0$, $T=212$).

The attractor shown in Fig. 13 is obtained for the single-switch scheme with a high value of $T=212$. In this case, the magnitude of kicking, ε_1, is set to $\varepsilon_1=0.787$ by choosing $R_1=3020\ \Omega$ in Fig. 2. Note that, as was seen in the corresponding numerical simulation of Fig. 8, the arms of the attractor in Fig. 13 are pressed down. By lowering the value of T, attractors with more visible structures are obtained as shown in Figs. 14 and 15. The one in Fig. 14 is obtained for the single-switch scheme with $T=60$ and $\varepsilon_1=0.787$ ($R_1=3020\ \Omega$). The attractor shown in Fig. 15 is obtained for the double-switch scheme with $T=112$, $\varepsilon_1=0.526$ ($R_1=2020\ \Omega$), and $\varepsilon_2=0.398$ ($R_2=2000\ \Omega$).

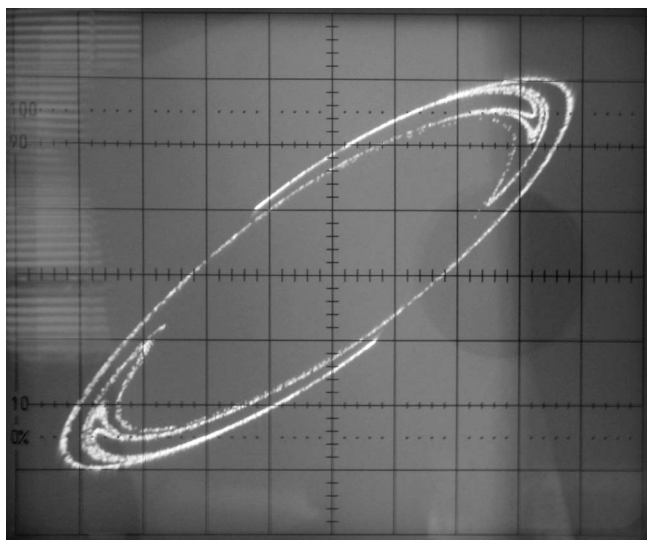

FIG. 14. Time-T map for a single-switch case rank 1 attractor from experimental simulations: smooth case ($\varepsilon_1=0.787$, $\varepsilon_2=\varepsilon_3=0$, $T=60$).

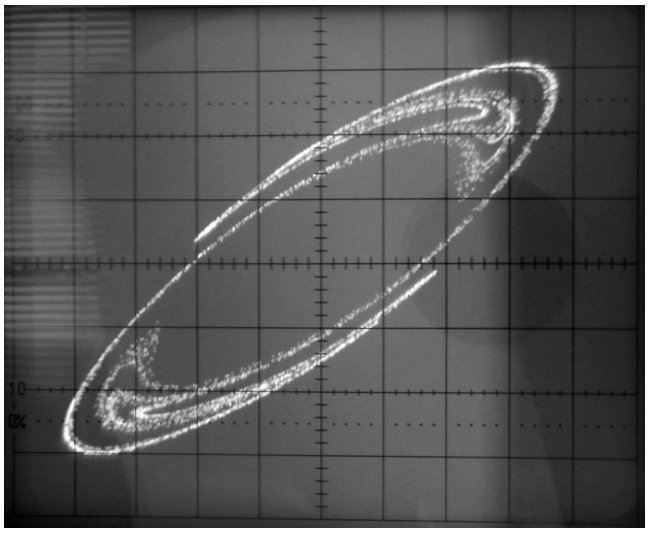

FIG. 15. Time-T map for a two-switch case rank 1 attractor from experimental simulations: smooth case ($\varepsilon_1=0.526$, $\varepsilon_2=0.398$, $\varepsilon_3=0$, $T=112$).

B. Piecewise linear case

The physical circuit implementation of the PWL resistor can, in general, be considered more feasible due to the fact that, unlike the case of smooth nonlinearity, it requires no analog multipliers but passive resistors and operational amplifiers only. Such a circuit realization of a three-segment PWL resistor is shown in Fig. 16. In this realization, high performance current feedback operational amplifiers are used. The passive element values for the circuit of Fig. 16 are chosen to be

$$R_a = 1.5\ \text{k}\Omega, \quad R_b = 1.7\ \text{k}\Omega, \quad R_m = 5.3\ \text{k}\Omega, \tag{35}$$

corresponding to

$$m_0 = -0.88, \quad m_1 = -0.4. \tag{36}$$

With this choice of parameters, the experimentally obtained non-Hopf limit cycle that is to be kicked is shown in Fig. 17. The attractor shown in Fig. 18 is experimentally obtained for the single-switch and high-T case where $\varepsilon_1=0.787$ ($R_1=3020\ \Omega$) and $T=155$. The attractor shown in Fig. 19 is for the single-switch and low-T case where $\varepsilon_1=0.66$ ($R_1=2410\ \Omega$) and $T=82$. For the double-switch case, R_1 and R_2 are set to 2410, and 2200 Ω, corresponding to $\varepsilon_1=0.66$ and $\varepsilon_2=0.36$, respectively. The chaotic attractor obtained in this case is for $T=75$ and shown in Fig. 20. Once again, in the high-T case, the arms of the attractors are radially pressed down to give it the look of a simple closed curve.

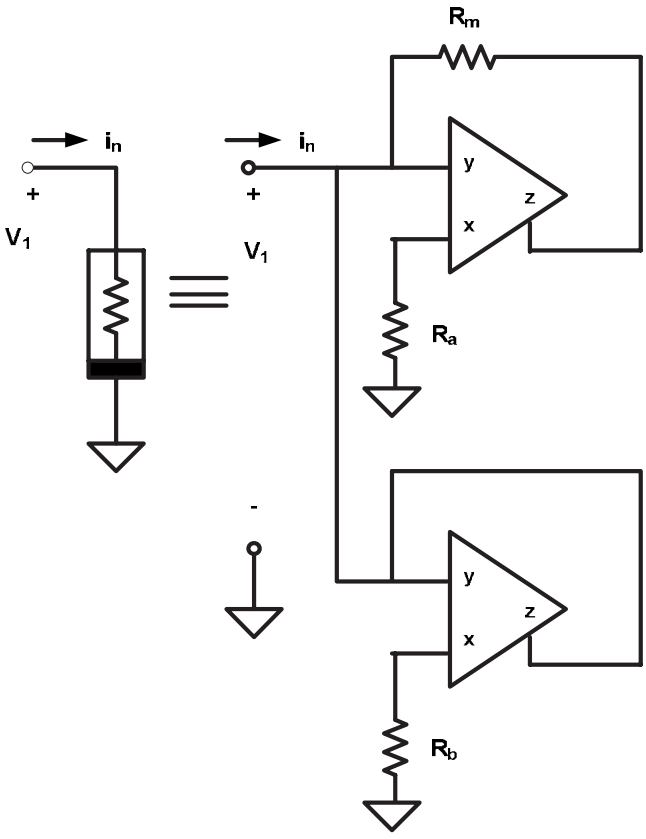

FIG. 16. A three-segment PWL resistor implementation.

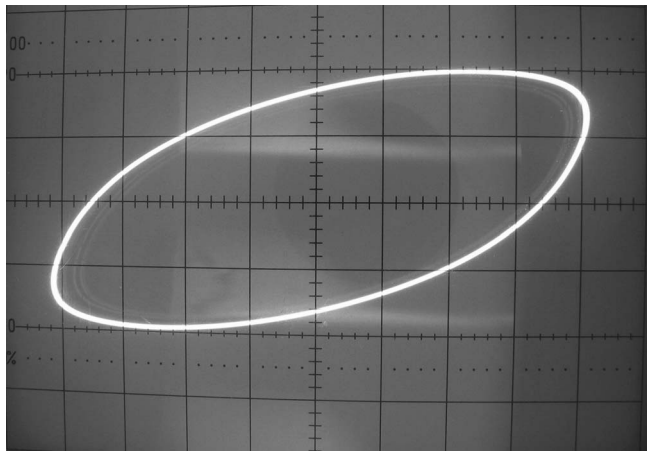

FIG. 17. A non-Hopf limit cycle from experimental simulations ($\varepsilon_i=0$).

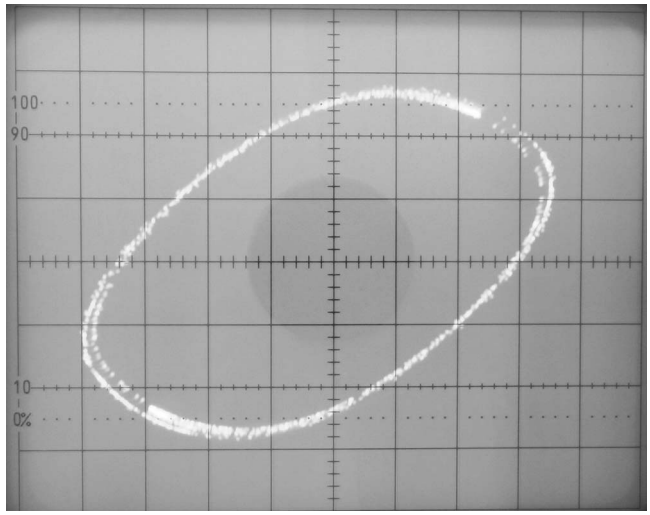

FIG. 18. Time-T map for a single-switch case rank 1 attractor from experimental simulations: PWL case ($\varepsilon_1=0.787$, $\varepsilon_2=\varepsilon_3=0$, $T=155$).

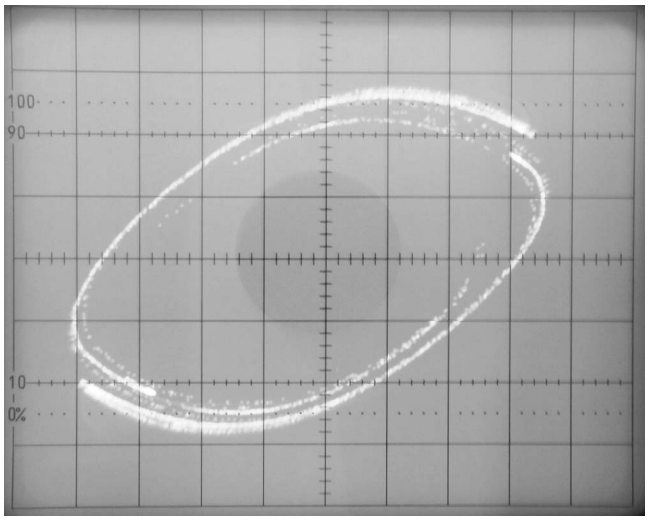

FIG. 19. Time-T map for a single-switch case rank 1 attractor from experimental simulations: PWL case ($\varepsilon_1=0.66$, $\varepsilon_2=\varepsilon_3=0$, $T=82$).

VI. CONCLUSION

In this paper, we have provided the first experimental proof of rank 1 chaos by using a switch-controlled Chua circuit. Both the smooth and the PWL cases have been investigated under different kicking schemes. In the smooth case, first, a weakly stable Hopf limit cycle coming out of a fixed point is generated. Then, under the guidance of the theory, by following a recipe-like procedure, this limit cycle is subjected to periodic kicks to obtain rank 1 attractors. The theory is also applicable in the case of arbitrary limit cycles. This makes it possible to obtain chaotic attractors in systems where the employed nonlinearity is not smooth. The generic setting of the theory is satisfied by adding externally controlled switches to the original circuit.

Even though the theory is equally applicable to smooth nonlinearity and PWL cases, each case has its own advantages and disadvantages. The advantage in the case of smooth nonlinearity is that, for this case, the theory provides a recipe-like procedure where the precise analytical computations for the emergence of chaos can easily be carried out (see Sec. III B). Therefore, in the smooth case, it is easier to follow the guidance of the theory, and hence to explicitly know in what manner to control the system parameters to generate chaos. However, the disadvantage in this case is the fact that the physical realization of the circuit can be relatively more difficult. As for the PWL case, one advantage is the ease of physical circuit realization. Nonetheless, the main difficulty in this case is that, currently, there is no recipe-like procedure available from which explicit analytical conditions for chaos can be derived. Despite this relative difficulty, the plethora of PWL systems in practice makes them a natural target for the application of the theory of rank 1 chaos.

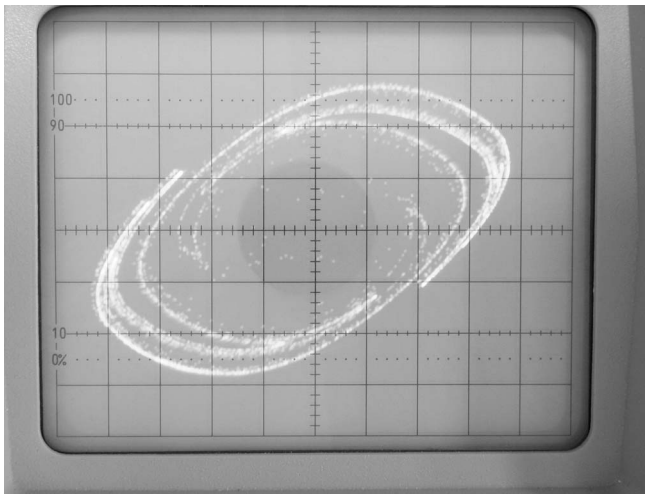

FIG. 20. Time-T map for a two-switch case rank 1 attractor from experimental simulations: PWL case ($\varepsilon_1=0.66$, $\varepsilon_2=0.36$, $\varepsilon_3=0$, $T=75$).

It is also worth noting that the results of the experimental simulations are in perfect agreement with the predictions of the theory. It also seems that the geometric complexity of the resulting attractors increases with the number of switches employed. Another point worth mentioning here is that the width of the applied pulses p_0 is not crucial (other than practical concerns for the physical switches used) as long as it is followed by a much longer relaxation interval, i.e., $T_0 \gg p_0$. For more background information on the theory of rank 1 chaos and its potential applications to circuits and systems, we refer the reader to a recent tutorial paper.[18]

ACKNOWLEDGMENTS

This project was partially supported by The Scientific and Technological Research Council of Turkey (TUBITAK) under Grant No. 106E093.

[1] Q. Wang and A. Oksasoglu, Int. J. Bifurcation Chaos Appl. Sci. Eng. **15**, 83 (2005).
[2] A. Oksasoglu and Q. Wang, Int. J. Bifurcation Chaos Appl. Sci. Eng. **16**, 2659 (2006).
[3] A. Oksasoglu, D. Ma, and Q. Wang, Int. J. Bifurcation Chaos Appl. Sci. Eng. **16**, 3207 (2006).
[4] A. Oksasoglu and Q. Wang, "Chaos in switch-controlled Chua's circuit," J. Franklin Inst. (unpublished).
[5] Q. Wang and L.-S. Young, Commun. Math. Phys. **218**, 1 (2001).
[6] D. Wang and L.-S. Young, J. Anal. Math. **167**, 349 (2008).
[7] D. Wang and L.-S. Young, Commun. Math. Phys. **225**, 275 (2002).
[8] M. Jakobson, Commun. Math. Phys. **81**, 39 (1981).
[9] M. Benedicks and L. Carleson, J. Anal. Math. **133**, 73 (1991).
[10] L. O. Chua, J. Circuits Syst. Comput. **4**, 117 (1994).
[11] G. Q. Zhong, IEEE Trans. Circuits Syst., I: Fundam. Theory Appl. **41**, 934 (1994).
[12] D. Wang and L.-S. Young, Commun. Math. Phys. **240**, 509 (2002).
[13] J. Guckenheimer and P. Holmes, *Nonlinear Oscillations, Dynamical Systems and Bifurcations of Vector Fields*, 5th ed. (Springer-Verlag, New York, 1997).
[14] L.-S. Young, J. Stat. Phys. **108**, 733 (2002).
[15] H. G. Schuster and W. Just, *Deterministic Chaos: An Introduction*, 4th ed. (Wiley-VCH, Weinheim, 2005), Chap. 2.2.
[16] A. Venkatesan, S. Parthasarathy, and M. Lakshmanan, Chaos, Solitons Fractals **18**, 891 (2003).
[17] S. Parthasarathy and K. Manikandakumar, Chaos **17**, 043120 (2007).
[18] Q. Wang and A. Oksasoglu, Int. J. Bifurcation Chaos Appl. Sci. Eng. **18**, 1261 (2008).